Journal of Materials Chemistry C

Accepted Manuscript

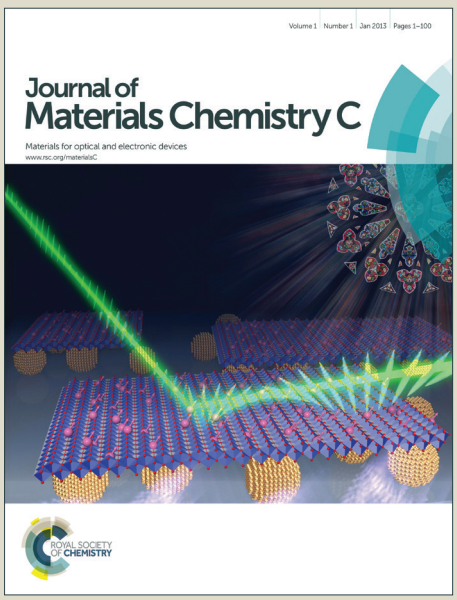

ROYAL SOCIETY OF CHEMISTRY

www.rsc.org/materialsC

Photophysical Properties of Ionic Liquid-Assisted Porphyrin Nanoaggregate-Nickel Phthalocyanine Conjugates and Singlet Oxygen Generation

Sadananda Mandal, Simanta Kundu, Santanu Bhattacharyya, and Amitava Patra*

Department of Materials Science, Indian Association for the Cultivation of Science, Kolkata, 700 032, India

*Authors to whom correspondence should be addressed; electronic mail: **msap@iacs.res.in** Phone: (91)-33-2473-4971, Fax: (91)-33-2473-280

Abstract

In this report, we demonstrate the formation of ionic liquid (IL)-assisted zinc octaethylporphyrin (ZnOEP) nanoaggregate which is confirmed by field emission scanning electron microscopy (FE-SEM) and atomic force microscopy (AFM) studies. A large red shifted emission of ZnOEP nanoaggregate in comparison to ZnOEP in DCM is confirmed the H aggregation which is due to intermolecular porphyrin-porphyrin (such as π-π/hydrophobic) interactions. The steady state and time resolved spectroscopic studies unambiguously confirm the H-aggregation formation of porphyrin molecules during nanoaggregate formation. The significant quenching of fluorescence spectrum and the shortening of decay time of porphyrin nanoaggregate imply an efficient (89%) energy transfer from porphyrin nanoaggregate to phthalocyanine. Furthermore, the emission band observed at 1270 nm, unambiguously confirms the singlet oxygen ($^1O_2$) generation from ZnOEP nanoaggregate which opens up further prospect in designing new IL-assisted porphyrin nanoaggregate for the application in photodynamic therapy.

Introduction

During the last decades, significant attention has been paid on aggregated nano-structures of various organic molecules to find out potential applications in photodynamic cancer therapies, artificial light harvesting, opto-electronic devices and various sensor technologies.[1-8] In particular, porphyrinoids-(free base porphyrins or metalloporphyrins) based nanostructures due to π-π stacking interactions, are of great interest for versatile applications in sensing, light harvesting, photocatalytic and organic photovoltaic for their excellent photophysical, photochemical, electrochemical properties.[9-11] Hasobe *et al.* have demonstrated that porphyrin-based nanoarchitectures are suitable for light energy conversion.[12, 13] Recently, they have synthesized CTAB-assisted TiO_2 doped zinc meso tetra(4-pyridyl) porphyrin hexagonal nanocylinders which exhibit efficient hydrogen evolution under visible light irradiation.[14] McHale and his co-workers have reported that porphyrin-based self-assembled structures have potential use in light harvesting and solar cell systems. Furthermore, surfactant-assisted nanospheres and nanorods of zinc meso-tetra(4-pyridyl)porphyrins have also been reported recently, which are being used for photocatalysis.[15-17] The tuning factors of the porphyrin aggregation in aqueous solution depend on the structure of porphyrin, concentration, pH and counter ions of inorganic salts in the medium.[18] Furthermore, the aggregation behavior of porphyrin in aqueous solution can be controlled by IL. Wu *et al.* have reported the J- aggregation behavior of diprotonated tetrakis(4-sulfonatophenyl) porphyrin in aqueous solution in the presence of the hydrophilic IL 1-butyl-3-methylimidazolium tetrafluoroborate.[19] Zhang *et al.* have investigated the self-assembly and supramolecular chirality of a dianionic tetrakis(4-sulfonatophenyl) porphyrin in the presence of 1-alkyl-3-methylimidazolium tetrafluoroborate. In addition, Pandey and his co-workers have reported the J-aggregation of mesotetrakis(4-sulfonatophenyl) porphyrin in an IL solution by varying the amount of acid concentration and poly(ethylene glycol).[20, 21] All

the preceding examples of IL-assisted porphyrin aggregation clearly demonstrate that IL plays an important role for the porphyrin aggregation. ILs are widely used as solvent, reactant, capping or templates in the synthesis of nanostructure materials with improved properties because of their unique range in liquid state, good dissolving ability, and high thermal stability, high ionic conductivity and non-flammability.[22-28] The supramolecular assembled structures of porphyrin molecules are governed by the various non-covalent interactions, such as hydrogen bonding, π−π stacking, hydrophobic and electrostatic interactions, and van der Waals forces, etc.[29-33] The supramolecular aggregations are mainly J-type (offset-stack or step like arrangement) and H-type (face-to-face arrangement) aggregates, which have unique electronic and spectroscopic properties due to their high structural order.[34]

Recently, zirconium / hafnium porphyrin and phthalocyanine complexes are being used for solar cell devices because porphyrins have strong blue absorption for B band and phthalocyanine has strong absorption in red for Q band, as a result combination of two are excellent candidates for solar light collection.[35] Photophysical properties of porphyrin-phthalocyanine conjugated system have been well studied to date in molecular state.[36-38] It is already demonstrated that CdSe QDs can be used to sensitize phthalocyanine (Pc4) via a resonance energy transfer to generate single oxygen for PDT applications.[39] Furthermore, singlet oxygen generation in photosensitizer doped polymer or silica nanostructures and carbon nanotube photosensitizer conjugate systems have been reported in some recent publications.[40-48] To the best of our knowledge, there is no report on singlet oxygen generation from porphyrin nanoaggregate or porphyrin-phthalocyanine nano-composites which could be useful for photodynamic therapy. Thus, an interesting challenge is to design porphyrin nanoaggregate -phthalocyanine conjugates and understand their photophysical properties.

In this work, we describe a system where Ni-phthalocyanine (NiPc) molecules are attached with IL-assisted ZnOEP nanoaggregate. H-type aggregation of porphyrin molecules are observed during nanoaggregate formation in presence of IL. An efficient energy transfer from porphyrin nanoaggregate to NiPc is successfully demonstrated. Again, singlet oxygen generation from porphyrin nanoaggregate has been investigated by phosphorescence spectra at the near infra red (NIR) region which might open up further prospect in designing new IL assisted porphyrin nanoaggregate for the application in photodynamic therapy.

Materials

Zinc octaethylporphyrin (Aldrich) [ZnOEP], nickel(II) phthalocyanine-tetrasulfonic acid tetrasodium salt (NiPC) [Aldrich], distilled tetrahydrofuran (THF) [MERCK], dichloromethane (DCM) [MERCK], cetyltrimethylammonium bromide (CTAB) [Alfa Aesar], sodium dodecyl sulfate (SDS) [Aldrich], de-ionized water (MERCK), deuterium dioxide (D_2O) [Aldrich], 1-methyl imidazole (Aldrich) and 1-bromohexadecane (SRL) were used as received for our synthesis. Scheme 1 shows the molecular structures of ZnOEP, NiPC and 1-hexadecyl-3-methylimidazolium bromide.

Experimental Section and Instrumentation

Synthesis of IL: The IL, 1-hexadecyl-3-methylimidazolium bromide ([HDMIm]Br) was prepared by a reported method using microwave irradiation in a mixture of 1-methyl imidazole and 1-bromohexadecane.[27, 49] The prepared IL was then purified by re-crystallization and dried in a vacuum and characterized by 300MHz ^{1}H NMR spectroscopy and ESI mass spectroscopy and the data agreed well with the previously reported values.[49, 50] Before using the IL, it was dried under high vacuum at 60^o C to evaporate the water.

Synthesis of IL-Assisted ZnOEP Nanoaggregate**:** The porphyrin nanoaggregate was synthesized by simple miniemulsion method.[51, 52] ZnOEP was properly dissolved in DCM to

maintain the 100 μM concentration of ZnOEP. A 500 μL aliquot of this DCM solution was rapidly injected into 2.75 mg of IL containing 10 mL of double distilled water under vigorous stirring for 10-15 minutes followed by ultrasonication for another 15 minutes to form stable miniemulsion containing small droplets of the ZnOEP solution. The DCM solvent was then evaporated by partial vacuum evaporation for 1 hour at 65^{o} C. Finally, we obtained a stable aqueous solution of ZnOEP nanoaggregate, which was stable for a week. CTAB- and SDS-assisted ZnOEP nanoaggregates were synthesized following the similar miniemulsion method.[53] The uncapped ZnOEP nanoaggregates were synthesized by re-precipitation method.[54-56]

Characterization: The morphological characters and sizes of ZnOEP NP were measured by Field Emission Scanning Electron Microscopy (FE-SEM, JEOL, JSM-6700F and Atomic Force Microscopy (AFM, VEECO, dicp-II). Room temperature optical absorption spectra were taken by a UV-vis spectrophotometer (SHIMADZU). Room temperature photoluminescence spectra were recorded by a Fluoromax-P (HORIBA JOBIN YVON) photoluminescence spectrophotometer. For the time correlated single photon counting (TCSPC) measurements, the samples were excited at 375 nm using a pico-second diode laser (IBH Nanoled-07) in an IBH Fluorocube apparatus. The typical full width at half maximum (FWHM) of the system response using a liquid scatter was about 90 ps. The repetition rate was 1 MHz. The fluorescence decays were collected at a Hamamatsu MCP photomultiplier (C487802). The fluorescence decays were analyzed using IBH DAS6 software. The following equation was used to analyze the experimental time resolved fluorescence decays, $P(t)$;[57]

$$P(t) = b + \sum_{i}^{n} \alpha_i \exp(-\frac{t}{\tau_i}) \qquad (1)$$

here, n is a number of discrete emissive species, b is a baseline correction ("dc" offset), and α_i and τ_i are pre-exponential factors and excited-state fluorescence lifetimes associated with the i^{th} component, respectively. For multi-exponential decays the average lifetime,$\langle\tau\rangle$, was calculated from the following equation,[58]

$$< \tau >= \sum_{i=1}^{n} a_i \tau_i \qquad (2)$$

Where $a_i = \alpha_i / \sum \alpha_i$ and a_i is contribution of the decay component. The phosphorescence spectra of singlet oxygen was monitored by using a Fluorolog-3 IHR spectrafluorometer (Jobin-Yvon) equipped with a NIR sensitive photomultiplier (Hamamatsu model: R5509-72) operated at a temperature of 277 K. For the phosphorescence measurement, IL assisted ZnOEP nanoaggregate were synthesized in D_2O media.

Results and Discussion

Structural Properties and Aggregation Behavior

Figure 1 shows the FE-SEM and AFM images of the IL-assisted ZnOEP nanoaggregate. These images unambiguously confirm the formation of spherical porphyrin nanoaggregate by the mini-emulsion method used in this study. The size distribution curve shows that the average diameter of ZnOEP nanoparticle is about 65 nm and the 3D AFM image shows that the average height of the particles is about 25 nm. The porphyrin nanoaggregate is formed due to the aggregation of porphyrin nanoparticles. A general mechanism of porphyrin nanoparticle formation is as follows: during the ejection of DCM solution of ZnOEP in the micellar solution of IL under the stirring condition, the solution divided into many stable small droplets of the ZnOEP solution by strong shearing force. The

porphyrin molecules are aggregated to form the nanoparticles in the hydrophobic micelle during the DCM solvent is evaporated by partial vacuum evaporation.

In general, porphyrins and metalloporphyrins feature two well-defined absorption regions, so-called a high-energy B (also known as Soret) and low-energy Q bands. Soret absorption band corresponds to $S_0 \rightarrow S_2$ electronic transitions, while Q bands correspond to $S_0 \rightarrow S_1$ electronic transitions.[59] Both the B and Q bands arise from π-π^* electronic transitions. Both S_1 and S_2 excitation states are splitted into the lower- and higher-level energy excited states due to 'H' (face-to-face) or 'J' (edge-to-edge) molecular aggregations.[60] According to the exciton coupling model,[61] the higher excited states are transitionally allowed in the case of H aggregation whereas lower excited states are transitionally allowed for J aggregation. As a result, hypsochromic and bathochromic shifts of absorption spectra occur for H and J aggregations, respectively. In this study, ZnOEP in DCM solvent shows a very sharp Soret band at 400 nm and Q bands at 530 nm and 567 nm (Figure 2), indicating a pure monomeric form.[62] However, the hypsochromic shifting of Soret band (by 11 nm) and bathochromic shifting of Q bands (by 17 nm and 25 nm) are observed for ZnOEP nanoaggregate. A large difference in the spectral shape of ZnOEP nanoaggregate and ZnOEP monomer is observed. In particular, the calculated FWHM values are 35 nm and 12 nm for ZnOEP nanoaggregate and ZnOEP monomer, respectively. The observed steady-state spectral changes (blue shift and spectral broadening) suggest that the ZnOEP molecules form the H-aggregated state due to the increment of local concentration of ZnOEP inside the IL micelle. One may expect that the spectral shifting is the result of solvatochromism because the monomeric porphyrin molecule and the porphyrin nanoaggregate are in the different solvents (molecular form in DCM and nanoparticles in aqueous solution, respectively). To clarify this point, absorption spectra of ZnOEP are taken in the different polar organic solvents in which the porphyrin molecules are soluble and exist as monomer (supporting information Figure S1). This

experiment suggests that the ZnOEP has positive solvatochromism property (i.e. bathochromic shift or red shift with increasing solvent polarity). Therefore, the blue shift (with respect to DCM solution) of ZnOEP in the nanoaggregate form (in water, more polar than DCM) unambiguously confirms the H-aggregation of ZnOEP.

Figure 2B shows the emission spectra of ZnOEP in DCM solution and ZnOEP nanoaggregate. Upon excitation of ZnOEP in DCM solvent at 375 nm, the fluorescence spectrum exhibits two emission bands at 572 nm (Q^*_{X00}) and 623 nm (Q^*_{X01}), which are the characteristic peaks of ZnOEP chromospheres in DCM solvent and in a good agreement with the previously reported data.[63] In the case of ZnOEP nanoaggregate the emission peaks at 597 nm (Q^*_{X00}) and 647 nm (Q^*_{X01}) are observed. A large red shifted emission (by 25 nm and 24 nm, correspondingly) and lower fluorescence intensity of ZnOEP nanoaggregate in comparison to ZnOEP in DCM are apparently due to the H aggregation (as discussed above) which is induced by intermolecular porphyrin-porphyrin (such as π-π/hydrophobic) interactions and the hydrophobic interaction between porphyrin and long hydrophobic chains of ILs. In this case, the emission spectrum of H aggregated ZnOEP nanoaggregate is red shifted with respect to the ZnOEP monomer because the emission occurs from the low energy excited state of H aggregated species which are transitionally forbidden, and it is further consisted with the previous report of H-aggregates of porphyrin-surfactant complexes by N. Periasamy et.al.[64]

In order to gain further information on the aggregation behavior of the ZnOEP in nanoaggregate form, the time resolved fluorescence spectra are taken at the excitation wavelength of 375 nm. Figure 3 depicts the photoluminescence decay profiles of ZnOEP in DCM and in nanoparticle form. In the case of ZnOEP in DCM, at the emission wavelength of 572 nm, the decay curve is fitted mono-exponentially with the life time of 1.48 ns, while at the emission wavelength of 623 nm the decay curve is fitted bi-exponentially with the decay

components of 1.48 ns (99%) and 9.80 ns (1%) and the average decay time is 1.56 ns. On the other hand, at the emission wavelength of 597 nm, the decay curve of ZnOEP nanoaggregate is fitted by tri-exponential with the decay component of 0.06 ns (90%), 0.66 ns (8%) and 2.02 ns (2%) and the average decay time is 0.15 ns. At the emission wavelength of 647 nm, the decay curve is also fitted by tri-exponential with the decay component of 0.11 ns (77%), 1.08ns (18%) and 3.68 ns (5%) and the average decay time is 0.46 ns. All the decay parameters are given in Table 1. After the formation of nanoaggregate, the average decay time of the ZnOEP decreases in both emission bands. The decrease of decay time of ZnOEP in nanoaggregate form confirms the H-aggregation of porphyrin molecules.[65]

Photoinduced Energy Transfer

In the present study, ZnOEP nanoaggregate -NiPC system has been designed by mixing NiPC molecules with the as synthesized ZnOEP nanoaggregate. The surface of ZnOEP nanoaggregate is positively charged due to the presence of positive imidazolium group of IL in the outside of the micelle and the NiPC is negatively charged due to the presence of sulfonate group which is confirmed by zeta potential study (supporting information Figure S2). Therefore, NiPCs are attached in the surface of ZnOEP nanoaggregate by electro-static interaction. Furthermore, the imidazolium group of IL may interact with the NiPC via stacking interaction because of their π-planar surface. Recently, Yaku and his co-workers reported that anionic phthalocyanines bind with the G-quadruplex via π-π stacking in spite of electrostatic repulsion.[66] To confirm the formation of IL-assisted ZnOEP nanoaggregate -NiPC composite, absorption spectra of NiPC (in the absence and in the presence of IL) have been taken. When increasing the concentration of IL, the absorption peak at 621 progressively disappears and two strong absorption peaks at 657 nm and 605 nm progressively appear (Figure 4). This spectral feature indicates the complex formation of NiPC with IL. Since, there is a perfect overlap between the emission spectra of porphyrin and

the absorption spectra of NiPC (Figure 5), thus the photoinduced energy transfer process from porphyrin nanoaggregate to NiPC is highly expected in this composite system. To investigate the energy transfer phenomena, steady state fluorescence and time resolved spectroscopic studies of this composite system have been carried out. Figure 6 shows the fluorescence emission spectra of IL-assisted ZnOEP nanoaggregate and ZnOEP nanoaggregate -NiPC systems with varying the concentration of NiPC at the excitation wavelength of 375 nm. An enhancement of the quenching efficiency of ZnOEP nanoaggregate in both emission bands is observed with increasing the concentration of NiPC. The values of fluorescence intensity quenching at the emission band of 597 nm are found to be 8, 25 and 38% for 4, 12 and 20 μM concentrations of NiPC, respectively. However, the values of fluorescence intensity quenching at the emission band of 647 nm are found to be 22, 56 and 70% for 4, 12 and 20 μM concentrations of NiPC, respectively. The fluorescence quenching is the indicative of the energy transfer from ZnOEP nanoaggregate to Ni-PC. To understand the energy transfer mechanism, the corresponding fluorescence decay times of ZnOEP nanoaggregate with and without NiPC are measured at both emission bands. Figure 7 shows the fluorescence decay curves of ZnOEP nanoaggregate with and without NiPC at both emissions [(A)-597 nm and (B)-647 nm]. All the decay curves are tri-exponentially fitted. At the emission wavelength of 647 nm, the average decay times of ZnOEP nanoaggregates are found to be 0.46 ns, 0.36 ns, 0.13 ns and 0.05 ns for the Ni-PC concentration of 0, 4, 12 and 20 μM, respectively (Table 1). At the emission wavelength of 597 nm, the average decay times of ZnOEP nanoaggregates are found to be 0.15 ns, 0.10 ns, 0.07 ns and 0.06 ns for the NiPC concentration of 0, 4, 12 and 20 μM, respectively (Table 2). The shortening of decay time of ZnOEP nanoaggregate in presence of NiPC confirms the energy transfer from porphyrin nanoaggregate to phthalocyanines. For the 20 μM concentration of NiPC, the calculated energy transfer efficiencies are 60% and 89% for the

emission wavelength of 597 and 647 nm, respectively. The energy transfer efficiency at 647 nm is higher than that of 597 nm which may be due to the better overlap between the absorption spectra of Ni-PC and second emission band of ZnOEP nanoaggregate (overlap integral values are 4.47 x 10^{-13} and 5.43 x 10^{-13} $M^{-1}cm^3$ for the emission wavelength of 597 and 647 nm, respectively).

To understand the importance of aggregated structures of porphyrin and the role of IL in the energy transfer process, we have done some control experiments. Since, IL is also soluble in DCM, hence, the NiPC is transferred to DCM using IL which is being used as a phase transferring agent. Steady state absorption, fluorescence and time resolved spectroscopic data's (supporting information Figure S3 and S4) show no electronic interaction between ZnOEP and NiPC in DCM solvent. Previously, we have also observed that no energy transfer occurs from poly (9-vinylcarbazole) (PVK) polymer to ZnOEP in DCM solvent, whereas, more than 90% energy transfer occurs when ZnOEP is aggregated in PVK nanoparticles.[67] Therefore, aggregation induced nanostructures of ZnOEP are the promising materials involved in the energy transfer process. The UV-vis, photoluminescence and fluorescence decay curves of ZnOEP nanoaggregate (synthesized by re-precipitation method) with and without NiPC are depicted in the supporting information Figures S5 and S6. It is found that the fluorescence intensity of ZnOEP nanoaggregate decreases rapidly but the decay time of the ZnOEP nanoaggregate decreases slightly with increasing NiPC concentration. The calculated energy transfer efficiencies are 54 % and 39% for the emission wavelength of 597 nm and 637 nm, respectively. In case of CTAB (a cationic surfactant)-assisted ZnOEP nanoaggregate, the energy transfer efficiencies are 13% and 18% for the corresponding emission bands. The absorption, fluorescence and fluorescence decay curves of CTAB-assisted ZnOEP nanoaggregate and ZnOEP-NiPC are given in the supporting information figures S7 and S8. The ZnOEP nanoaggregate are synthesised in presence of an

anionic surfactant, SDS. We do not observe any significant change in energy transfer from ZnOEP nanoaggregate to NiPC (supporting information Figure S9). Therefore, the above discussed results imply that IL has played an important role in the energy transfer process from porphyrin nanoaggregate to NiPC. It has been already reported that the stacking interaction occurs between anionic phthalocyanines with the G-quadruplexes.[66] Thus, we believe, the aromatic imidazolium group of the IL facilitates the π-π interaction with anionic NiPC, which enhances the energy transfer efficiency. More investigation is required to understand this phenomenon.

Photosensitization and Singlet Oxygen Generation

Besides, the significant energy donating property of the IL-assisted ZnOEP nanoaggregate to energy accepting NiPC molecules (discussed above), it can act as a very good singlet oxygen photosensitizer. The photoinduced singlet oxygen generation has been directly investigated by the phosphorescence spectra at the near infrared (NIR) region. Figure 8 shows the phosphorescence spectra of singlet oxygen at the excitation wavelength of 375 nm. The emission band observed at 1270 nm, unambiguously confirms the singlet oxygen generation from ZnOEP nanoaggregate. The ZnOEP nanoaggregate generates singlet oxygen by the following ways: during the excitation of ZnOEP nanoaggregate at 375 nm, the nanoaggregates are promoted to first excited singlet (S_1) state for Q-bands and second excited singlet (S_2) state for B-band. The particle goes down S_1 from S_2 state via internal conversion. Then, the nanoaggregate undergoes intersystem crossing from S_1 state to the triplet (T_1) state by a nonradiative relaxation process. The triplet state of the nanoparticle eventually transfers energy nonradiatively toward the triplet oxygen and converts to the singlet oxygen (Scheme 2a).[68] However, in the presence of NiPC, the singlet oxygen generation of ZnOEP nanoaggregate is reduced (curve b in Figure 8). It may be due to energy transfer from ZnOEP nanoaggregate to NiPC which reduces the population of triplet state of ZnOEP nanoaggregate

(Scheme 2b). Therefore, it can be plausibly concluded that ZnOEP nanoaggregate produces efficient amount of singlet oxygen which may open up further prospect in designing new IL-assisted porphyrin nanoaggregates for the application in photodynamic therapy.

Conclusion

In summary, we have successfully designed IL-assisted ZnOEP nanoaggregate which is confirmed from FE-SEM and AFM analysis. The steady state and time resolved spectroscopic investigation unambiguously confirm the H-aggregated state of porphyrin molecules during nanoaggregate formation. It is seen that no energy transfer takes place from porphyrin to phthalocyanine in an organic solvent while the efficient energy transfer (88.5%) takes place from IL-assisted ZnOEP nanoaggregate to the NiPC molecule due to close proximity by electrostatic as well as π-π interaction. Furthermore, the IL-assisted ZnOEP nanoaggregate are the better energy donor compared to the uncapped ZnOEP nanoaggregate and surfactant-assisted ZnOEP nanoaggregate due to π-π interaction between IL and NiPC. This remarkably high efficiency of energy transfer in the IL-assisted ZnOEP nanoaggregate - NiPC system opens up further prospects in potential applications as various photodriven devices. Since, the porphyrin nanoaggregate and the conjugate system can produce efficient amount of singlet oxygen, these systems may be useful for bio-imaging and therapeutic applications.

Acknowledgement

SERB-DST and "DAE-SRC Outstanding Investigator Award" are gratefully acknowledged for financial support. SM and SK thank CSIR and SB thanks IACS for awarding fellowship. Subrata Das is acknowledged for the technical assistance. Mr. Abhishek Bhattacharya (Department of Biochemistry, University of Calcutta) is acknowledged for measuring the phosphorescence spectra.

Supporting Information

†Electronic Supplementary Information (ESI) available: Tables T1, T2, UV-vis spectra, Zeta potential curves, Photoluminescence spectra, and Photoluminescence decay curves of different systems. See DOI: 10.1039/b000000x/.

References

1. J.-M. Lehn, *Science*, 2002, **295**, 2400-2403.
2. Q. Ding, Y.-E. Miao and T. Liu, *ACS Appl. Mater. Interfaces*, 2013, **5**, 5617-5622.
3. B. Khlebtsov, E. Panfilova, V. Khanadeev, O. Bibikova, G. Terentyuk, A. Ivanov, V. Rumyantseva, I. Shilov, A. Ryabova, V. Loshchenov and N. G. Khlebtsov, *ACS Nano*, 2011, **5**, 7077-7089.
4. S.-G. Chen, Y. Yu, X. Zhao, Y. Ma, X.-K. Jiang and Z.-T. Li, *J. Am. Chem. Soc.*, 2011, **133**, 11124-11127.
5. T. Hasobe, H. Imahori, P. V. Kamat, T. K. Ahn, S. K. Kim, D. Kim, A. Fujimoto, T. Hirakawa and S. Fukuzumi, *J. Am. Chem. Soc.*, 2004, **127**, 1216-1228.
6. C. M. Drain, G. Smeureanu, S. Patel, X. Gong, J. Garno and J. Arijeloye, *New J. Chem.*, 2006, **30**, 1834-1843.
7. H.-X. Ji, J.-S. Hu and L.-J. Wan, *Chem. Commun.*, 2008, 2653-2655.
8. K. Ogawa and Y. Kobuke, *BioMed Res. Int.*, 2013, **2013**, 125658-125668.
9. K. M. Kadish, K. M. Smith, R. Guilard and Editors, *The Porphyrin Handbook;* Eds.; Academic Press: San Diego, CA, 2000; **Vol. 6**, p 346.
10. H. Imahori, T. Umeyama, K. Kurotobi and Y. Takano, *Chem. Commun.*, 2012, **48**, 4032-4045.
11. C. M. Drain, A. Varotto and I. Radivojevic, *Chem. Rev.*, 2009, **109**, 1630-1658.
12. T. Hasobe, *Phys. Chem. Chem.Phys.*, 2010, **12**, 44-57.
13. T. Hasobe, *J. Phys.Chem. Lett.* 2013, **4**, 1771-1780.
14. T. Hasobe, H. Sakai, K. Mase, K. Ohkubo and S. Fukuzumi, *J. Phys. Chem. C*, 2013, **117**, 4441-4449.
15. P. Guo, P. Chen, W. Ma and M. Liu, *J.Mater. Chem.*, 2012, **22**, 20243-20249.
16. P. Guo, P. Chen and M. Liu, *ACS Appl. Mater. Interfaces*, 2013, **5**, 5336-5345.
17. S. Mandal, S. K. Nayak, S. Mallampalli and A. Patra, *ACS Appl. Mater. Interfaces*, 2014, **6**, 130-136.
18. S. C. Doan, S. Shanmugham, D. E. Aston and J. L. McHale, *J. Am. Chem. Soc.*, 2005, **127**, 5885-5892.
19. J.-J. Wu, N. Li, K.-A. Li and F. Liu, *J. Phys. Chem. B*, 2008, **112**, 8134-8138.
20. M. Ali, V. Kumar, S. N. Baker, G. A. Baker and S. Pandey, *Phys. Chem. Chem. Phys.*, 2010, **12**, 1886-1894.
21. P. Dutta, R. Rai and S. Pandey, *J. Phys. Chem. B*, 2011, **115**, 3578-3587.

22. X. Duan, J. Ma, J. Lian and W. Zheng, *CrystEngComm*, 2014, **16**, 2550-2559.
23. M. Antonietti, D. Kuang, B. Smarsly and Y. Zhou, *Angew. Chem., Int. Ed.*, 2004, **43**, 4988-4992.
24. Y.-J. Zhu, W.-W. Wang, R.-J. Qi and X.-L. Hu, *Angew. Chem., Int. Ed.*, 2004, **43**, 1410-1414.
25. J. Ma, L. Chang, J. Lian, Z. Huang, X. Duan, X. Liu, P. Peng, T. Kim, Z. Liu and W. Zheng, *Chem. Commun.*, 2010, **46**, 5006-5008.
26. J. G. Huddleston, A. E. Visser, W. M. Reichert, H. D. Willauer, G. A. Broker and R. D. Rogers, *Green Chem.*, 2001, **3**, 156-164.
27. S. Kundu, A. Kar and A. Patra, *J. Lumin.*, 2012, **132**, 1400-1406.
28. A. Kar, S. Kundu and A. Patra, *RSC Adv.*, 2012, **2**, 4879-4885.
29. L. A. Estroff and A. D. Hamilton, *Chem. Rev.*, 2004, **104**, 1201-1217.
30. J.-H. Ryu and M. Lee, *J. Am. Chem. Soc.*, 2005, **127**, 14170-14171.
31. M. Ikeda, M. Takeuchi and S. Shinkai, *Chem. Commun.*, 2003, 1354-1355.
32. E. Lee, J.-K. Kim and M. Lee, *Angew. Chem., Int. Ed.*, 2008, **47**, 6375-6378.
33. L. Chen, S. Revel, K. Morris and D. J. Adams, *Chem. Commun.*, 2010, **46**, 4267-4269.
34. M. Kasha, *Radiat. Res.*, 1963, **20**, 55-70.
35. I. Radivojevic, G. Bazzan, B. P. Burton-Pye, K. Ithisuphalap, R. Saleh, M. F. Durstock, L. C. Francesconi and C. M. Drain, *J. Phys. Chem. C*, 2012, **116**, 15867-15877.
36. Z. Zhao, T. Nyokong and M. D. Maree, *Dalton Trans.*, 2005, 3732-3737.
37. S. Tannert, E. A. Ermilov, J. O. Vogel, M. T. M. Choi, D. K. P. Ng and B. Röder, *J. Phys. Chem. B*, 2007, **111**, 8053-8062.
38. E. A. Ermilov, S. Tannert, T. Werncke, M. T. M. Choi, D. K. P. Ng and B. Roeder, *Chem. Phys.*, 2006, **328**, 428-437.
39. A. C. S. Samia, X. Chen and C. Burda, *J. Am. Chem. Soc.*, 2003, **125**, 15736-15737.
40. X. Shen, F. He, J. Wu, G. Q. Xu, S. Q. Yao and Q.-H. Xu, *Langmuir*, 2011, **27**, 1739-1744.
41. S. Bhattacharyya, M. K. Barman, A. Baidya and A. Patra, *J. Phys. Chem. C*, 2014, **118**, 9733-9740.
42. L. M. Rossi, P. R. Silva, L. L. R. Vono, A. U. Fernandes, D. B. Tada and M. S. Baptista, *Langmuir*, 2008, **24**, 12534-12538.

43. C.-Y. Chen, Y. Tian, Y.-J. Cheng, A. C. Young, J.-W. Ka and A. K. Y. Jen, *J. Am. Chem. Soc.*, 2007, **129**, 7220-7221.
44. M. Kuruppuarachchi, H. Savoie, A. Lowry, C. Alonso and R. W. Boyle, *Mol. Pharmaceutics*, 2011, **8**, 920-931.
45. S. Ishihara, J. Labuta, W. Van Rossom, D. Ishikawa, K. Minami, J. P. Hill and K. Ariga, *Phys. Chem. Chem. Phys.*, 2014, **16**, 9713-9746.
46. R. Chitta, A. S. D. Sandanayaka, A. L. Schumacher, L. D'Souza, Y. Araki, O. Ito and F. D'Souza, *J. Phys. Chem. C*, 2007, **111**, 6947-6955.
47. J. W. Walton, A. Bourdolle, S. J. Butler, M. Soulie, M. Delbianco, B. K. McMahon, R. Pal, H. Puschmann, J. M. Zwier, L. Lamarque, O. Maury, C. Andraud and D. Parker, *Chem. Commun.*, 2013, **49**, 1600-1602.
48. D. Brevet, M. Gary-Bobo, L. Raehm, S. Richeter, O. Hocine, K. Amro, B. Loock, P. Couleaud, C. Frochot, A. Morere, P. Maillard, M. Garcia and J.-O. Durand, *Chem. Commun.,* 2009, **45**, 1475-1477.
49. R. S. Varma and V. V. Namboodiri, *Chem, Commun.*, 2001, 643-644.
50. E. Dinda, S. Si, A. Kotal and T. K. Mandal, *Chem. - A Eur. J.*, 2008, **14**, 5528-5537.
51. X. Gong, T. Milic, C. Xu, J. D. Batteas and C. M. Drain, *J. Am. Chem. Soc.*, 2002, **124**, 14290-14291.
52. D. Tuncel and H. V. Demir, *Nanoscale*, 2010, **2**, 484-494.
53. L. Vurth, C. Hadad, S. Achelle, J. C. Garcia-Martinez, J. Rodriguez-Lopez and O. Stephan, *Colloid. Polym. Sci.*, 2012, **290**, 1353-1359.
54. S. Bhattacharyya, T. Sen and A. Patra, *J. Phys. Chem. C*, 2010, **114**, 11787-11795.
55. F. Kong, Y. M. Sun and R. K. Yuan, *Nanotechnology*, 2007, **18**, 265707/265701-265707/265705.
56. S. Mandal, S. Bhattacharyya, V. Borovkov and A. Patra, *J. Phys. Chem. C*, 2011, **115**, 24029-24036.
57. J. R. Lakowicz, *Principles of Fluorescence Spectroscopy*, 3rd ed.; Kluwer Academic/Plenum Publishers: New York, 1999; p 496.
58. S. Mandal, M. Rahaman, S. Sadhu, S. K. Nayak and A. Patra, *J. Phys. Chem. C*, 2013, **117**, 3069-3077.
59. K. M. Smith *Porphyrins and Metalloporphyrins*, Ed.; Elsevier: Amsterdam, 1975; p 910.
60. S. Arnold, W. B. Whitten and A. C. Damask, *Phys. Rev. B*, 1971, **3**, 3452-3457.

61. M. Kasha, H. R. Rawls and M. A. El-Bayoumi, *Pure Appl. Chem.*, 1965, **11**, 371-392.
62. V. V. Borovkov, J. M. Lintuluoto and Y. Inoue, *J. Am. Chem. Soc.*, 2001, **123**, 2979-2989.
63. O. Ohno, Y. Kaizu and H. Kobayashi, *J. Chem. Phys.*, 1985, **82**, 1779-1787.
64. N. C. Maiti, S. Mazumdar and N. Periasamy, *J. Phys. Chem. B*, 1998, **102**, 1528-1538.
65. S. Verma, A. Ghosh, A. Das and H. N. Ghosh, *J. Phys. Chem. B*, 2010, **114**, 8327-8334.
66. H. Yaku, T. Murashima, D. Miyoshi and N. Sugimoto, *Chem. Commun.*, 2010, **46**, 5740-5742.
67. S. Mandal, S. Bhattacharyya, V. Borovkov and A. Patra, *J. Phys. Chem. C*, 2012, **116**, 11401-11407.
68. P. N. Prasad, *Introduction to biophotonics*, John Wiley & Sons; Inc.: Hoboken, NJ, 2003; pp 203−249.

Table 1: Decay parameters of ZnOEP in DCM solution and in IL-assisted nanoaggregates at excitation wavelength of 375 nm.

Sample	Emission (nm)	τ_1 (ns) (a_1)	τ_2 (ns) (a_2)	τ_3 (ns) (a_3)	$<\tau>$ (ns)
ZnOEP in DCM	572	1.48 (1)	---	---	1.48
	623	1.48 (0.99)	9.81 (0.01)	---	1.56
IL assisted ZnOEP nanoaggregate	597	0.06 (0.90)	0.66 (0.08)	2.02 (0.02)	0.15
	647	0.11 (0.77)	1.08 (0.18)	3.68 (0.05)	0.46

Table 2: Decay parameters of IL-assisted ZnOEP nanoaggregate with varying concentrations of NiPC at excitation wavelength of 375 nm.

Sample	Emission (nm)	τ_1 (ns) (a_1)	τ_2 (ns) (a_2)	τ_3 (ns) (a_3)	$\langle\tau\rangle$ (ns)
ZnOEP nanoaggregate	597	0.06 (0.90)	0.66 (0.08)	2.02 (0.02)	0.15
	647	0.11 (0.77)	1.08 (0.18)	3.68 (0.05)	0.46
ZnOEP nanoaggregate + 4 μM Ni-PC	597	0.04 (0.93)	0.52 (0.05)	1.86 (0.02)	0.10
	647	0.09 (0.81)	0.99 (0.15)	3.55 (0.04)	0.36
ZnOEP nanoaggregate + 12 μM Ni-PC	597	0.03 (0.94)	0.42 (0.05)	1.79 (0.01)	0.07
	647	0.04 (0.92)	0.55 (0.06)	2.92 (0.02)	0.13
ZnOEP nanoaggregate + 20 μM Ni-PC	597	0.03 (0.95)	0.43 (0.04)	1.77 (0.01)	0.06
	647	0.02 (0.97)	0.46 (0.02)	2.64 (0.01)	0.05

Figure captions

Scheme 1: (A) Zinc octaethylporphyrin, (B) 1-hexadecyl-3-methylimidazolium bromide and (C) nickel(II) phthalocyanine-tetrasulfonic acid tetrasodium salt.

Scheme 2. Schematic representation of pathways of singlet oxygen generation.

Figure 1: Images of IL-assisted ZnOEP nanoaggregate (A) FE-SEM and (B) AFM images (3D).

Figure 2: (A) UV-vis spectra and (B) fluorescence spectra of ZnOEP (a) in DCM solution and (b) in nanoaggregates form.

Figure 3: Photoluminescence decay curves of ZnOEP at the excitation wavelength of 375 nm (a) ZnOEP in DCM (λ_{em}=572 nm), (b) ZnOEP in DCM (λ_{em}= 623 nm), (c) ZnOEP nanoaggregate in water (λ_{em}=597 nm) and (d) ZnOEP nanoaggregate in water (λ_{em}=623 nm).

Figure 4: Absorption spectra of NiPC at different concentrations of IL.

Figure 5: Overlap spectra between absorption of NiPC and emission of ZnOEP nanoaggregate.

Figure 6: Photoluminescence spectra of ZnOEP nanoaggregate in presence of different concentrations of NiPC.

Figure 7: Photoluminescence decay curves of ZnOEP nanoaggregate at the emission wavelength of (A) 597 nm and (B) 637 nm, in presence of different concentrations of NiPC (a) 0 μM, (b) 4 μM, (c) 12 μM and (d) 20 μM NiPC (Excitation wavelength at 375 nm).

Figure 8: Phosphorescence spectra of singlet oxygen (a) IL-assisted ZnOEP nanoaggregate (b) IL-assisted ZnOEP nanoaggregate with NiPC at the excitation wavelength of 375 nm.

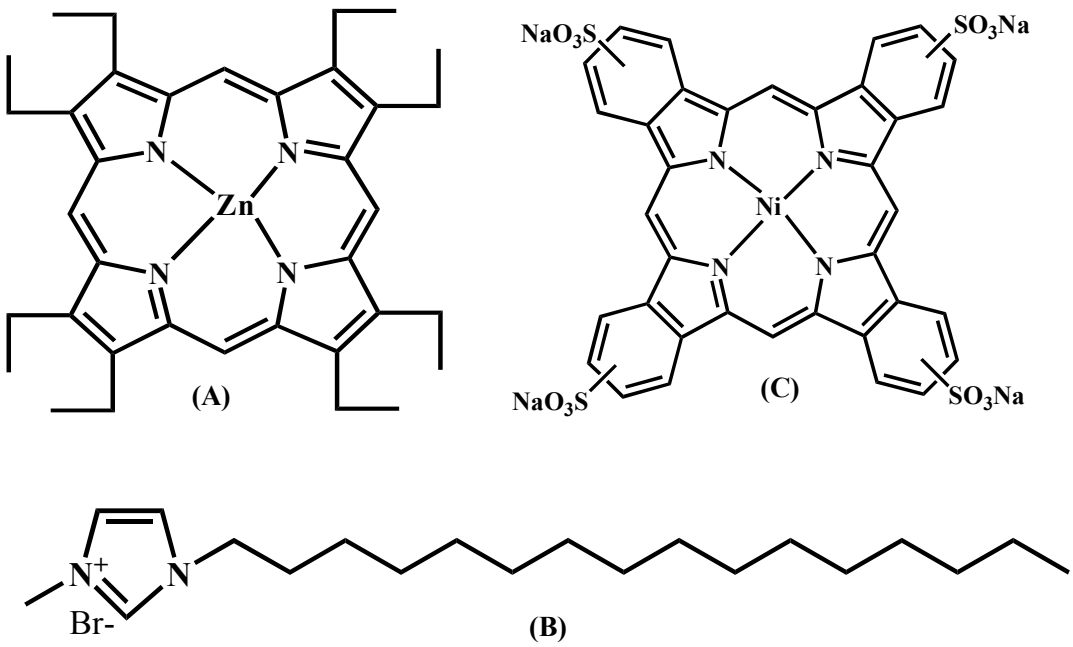

Scheme 1: (A) Zinc octaethylporphyrin, (B) 1-hexadecyl-3-methylimidazolium bromide and (C) nickel(II) phthalocyanine-tetrasulfonic acid tetrasodium salt.

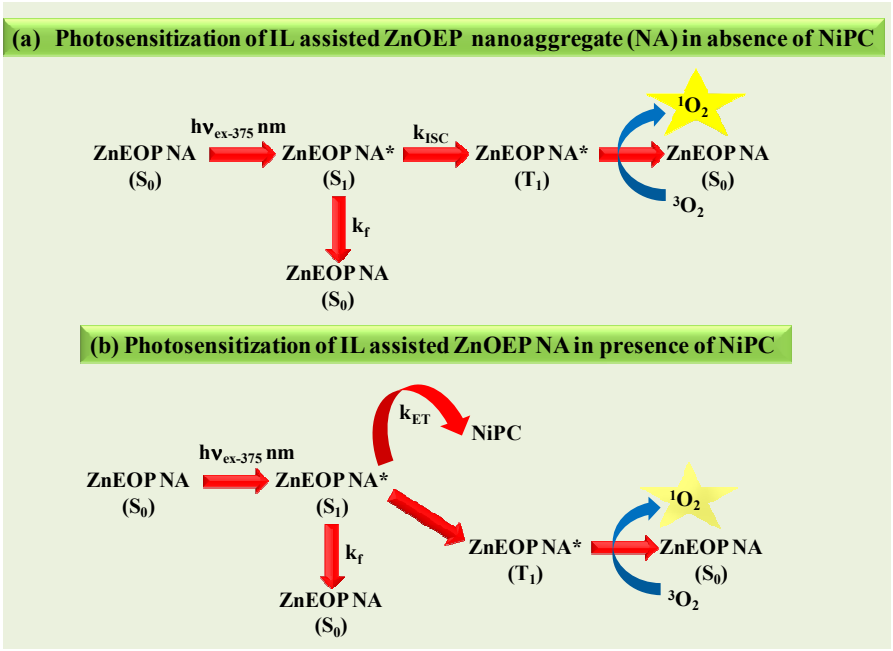

Scheme 2. Schematic representation of pathways of singlet oxygen generation.

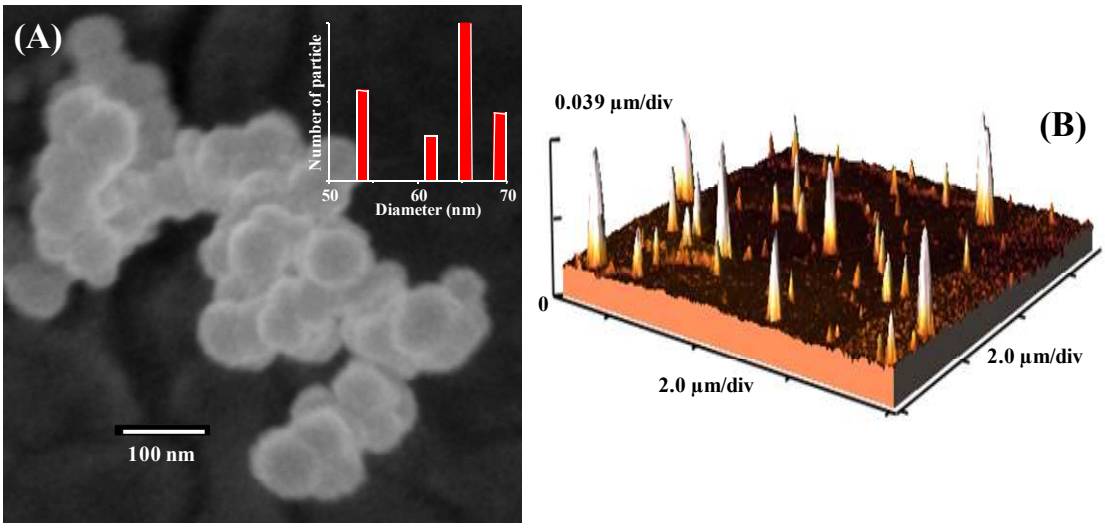

Figure 1: Images of IL assisted ZnOEP nanoaggregate (A) FE-SEM and (B) AFM images (3D) respectively.

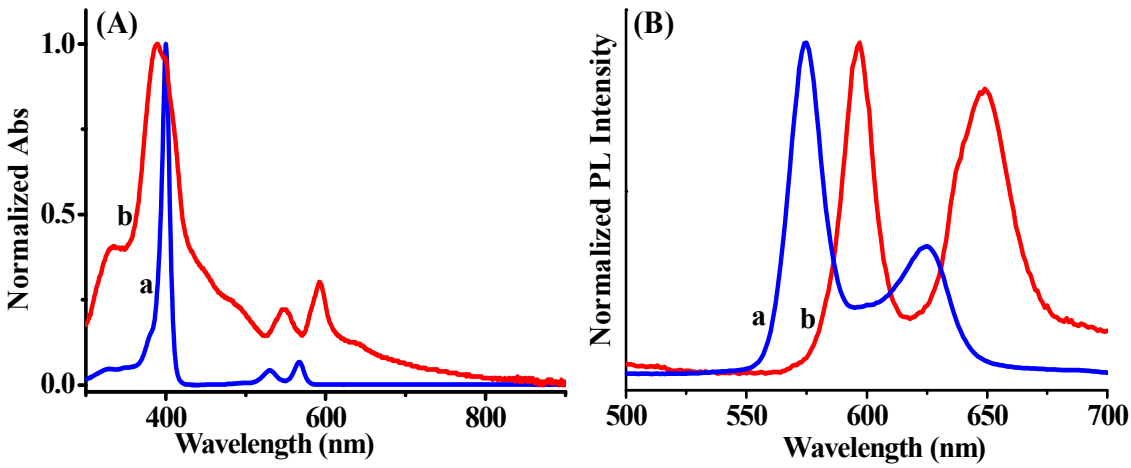

Figure 2: (A) UV-vis spectra and (B) fluorescence spectra of ZnOEP (a) in DCM solution and (b) nanoaggregate form.

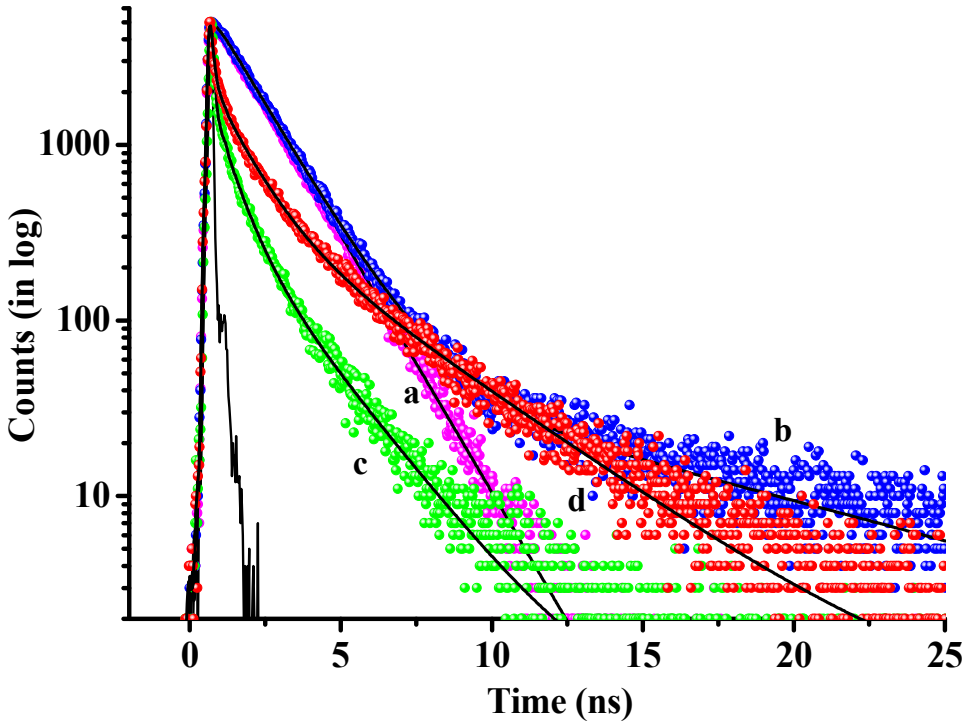

Figure 3: Photoluminescence decay curves of ZnOEP at the excitation wavelength of 375 nm (a) ZnOEP in DCM (λ_{em}=572 nm), (b) ZnOEP in DCM (λ_{em}= 623 nm), (c) ZnOEP nanoaggregate in water (λ_{em}=597 nm) and (d) ZnOEP nanoaggregate in water (λ_{em}=623 nm).

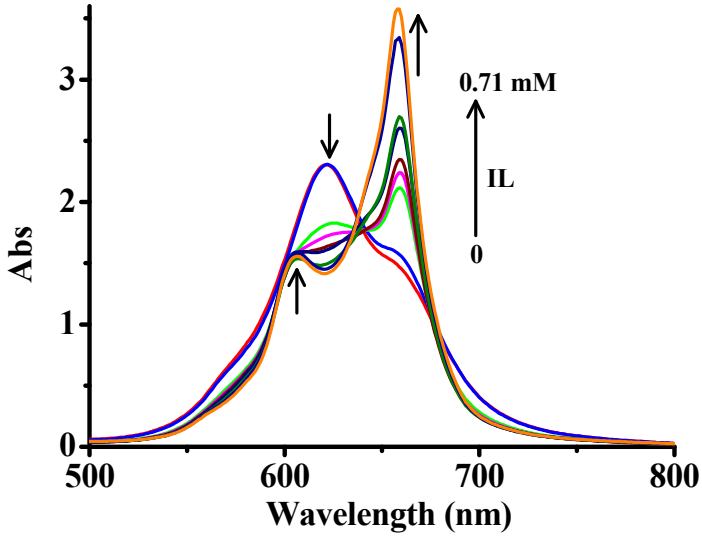

Figure 4: Absorption spectra of NiPC at different concentrations of IL.

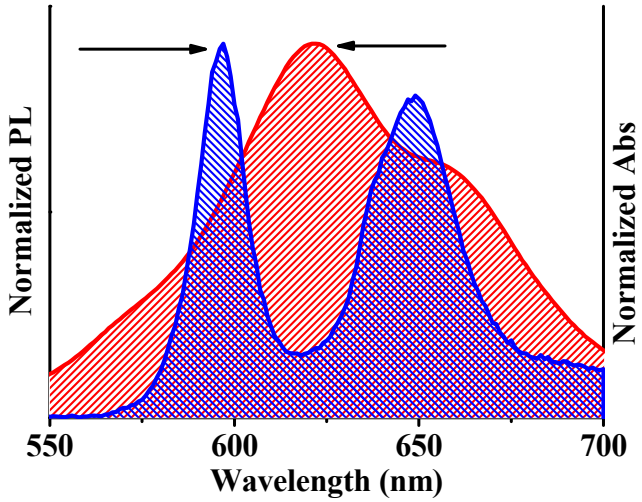

Figure 5: Overlap spectra between absorption of NiPC and emission of ZnOEP nanoaggregate

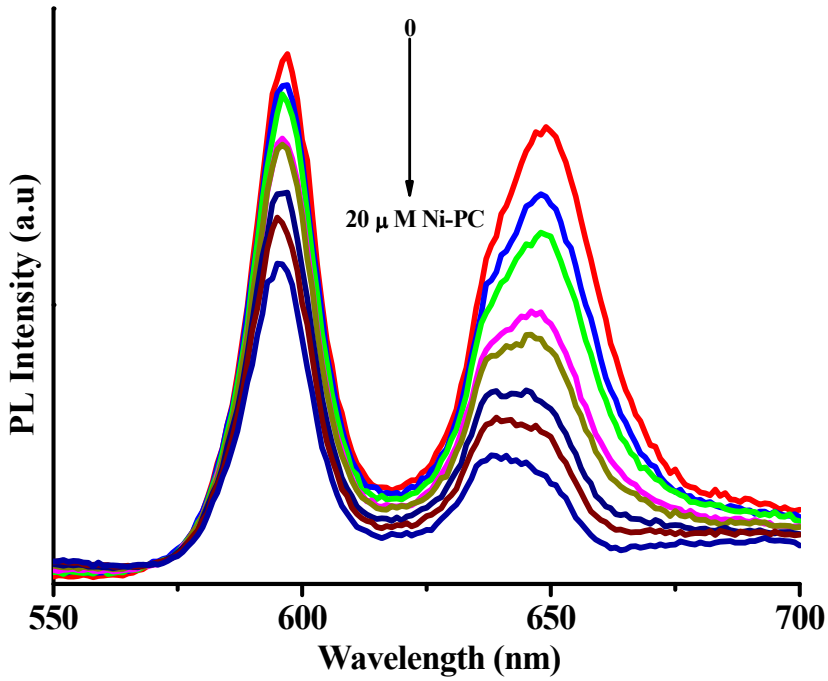

Figure 6: Photoluminescence spectra of ZnOEP nanoaggregate in presence of different concentrations of NiPC.

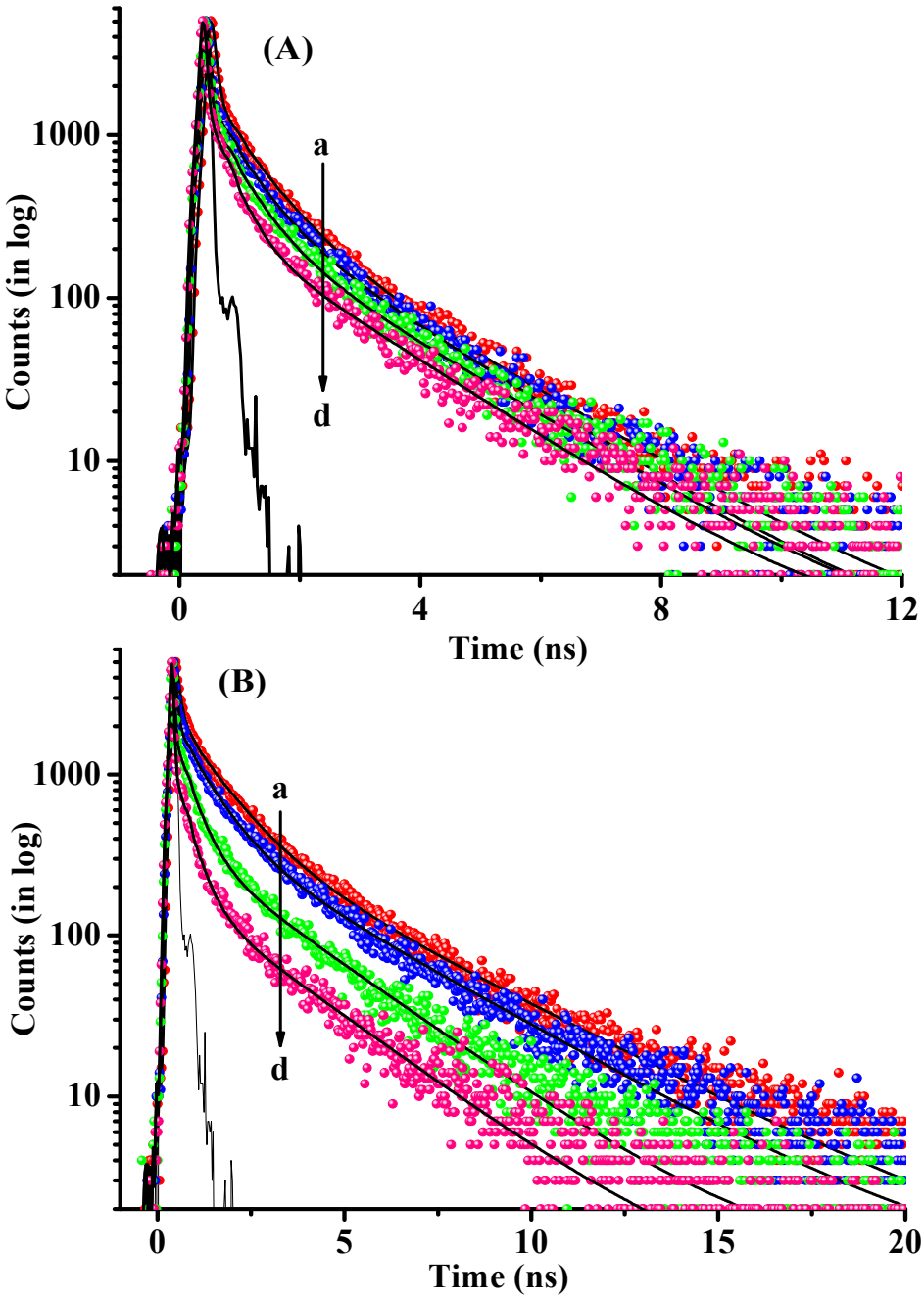

Figure 7: Photoluminescence decay curves of ZnOEP nanoaggregate at the emission wavelength of (A) 597 nm and (B) 637 nm, in presence of different concentrations of NiPC (a) 0 μM, (b) 4 μM, (c) 12 μM and (d) 20 μM NiPC (Excitation wavelength at 375 nm).

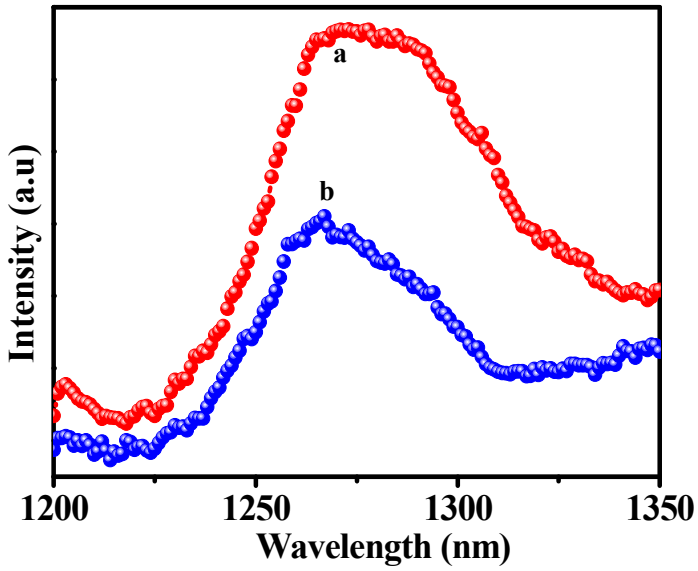

Figure 8. Phosphorescence spectra of singlet oxygen (a) IL-assisted ZnOEP nanoaggregate (b) IL-assisted ZnOEP nanoaggregate with NiPC at the excitation wavelength of 375 nm.

TOC

Porphyrin nanoaggregates for singlet oxygen generation